Available online at www.sciencedirect.com
SCIENCE DIRECT
Journal of Power Sources 154 (2006) 35–41
JOURNAL OF POWER SOURCES
www.elsevier.com/locate/jpowsour

Performance characteristics of micro single-chamber solid oxide fuel cell: Computational analysis

Chan-Yeup Chung, Yong-Chae Chung *

Department of Ceramic Engineering, Hanyang University, Seoul 133-791, Republic of Korea

Received 18 January 2005; accepted 28 March 2005
Available online 20 June 2005

Abstract

Performance characteristics of micro, single-chamber, intermediate temperature solid oxide fuel cell (IT–SOFC) has been successfully evaluated by computational simulation based on macro modelling. The system has composite electrodes that are alternately placed on the ceria-based electrolyte. The polarization curve is obtained through the series of computational processes for structural parameters such as distance between the anode and the cathode and the thickness of the electrolyte. Also, the effect of the inflow direction of fuel–air mixture on the performance of the fuel cell is quantitatively investigated.

Keywords: Micro single-chamber intermediate temperature solid oxide fuel cell; Computer simulation; Macro modelling; Polarization curve prediction

1. Introduction

The solid oxide fuel cell (SOFC) is highly efficient energy-conversion system that converts chemical energy to electrical energy. It can utilize hydrocarbons such as CH_4, C_2H_6 and C_3H_8 and CO besides H_2 as a fuel source. No additional fuel-reformer system is required because of the high operation temperature. The SOFC can be applied to versatile power generation systems, such as stationary power supplies, auxiliary power sources for automobiles and military applications. Research has been mainly focused on the fabrication of various forms of SOFC, e.g., tubular and planar types, for commercial applications. Experimental attempts have also been made, [1,2] to develop develop micro SOFCs (μSOFCs) as power sources of portable equipment and MEMS application [1,2]. To achieve stability and economical efficiency, intermediate temperature SOFCs (IT–SOFCs) with ceria-based electrolyte have been proposed [3–6]. Materials such as stainless steel can be employed as a bipolar plate in IT–SOFC systems and, consequently, low processing cost can be attained. Gas sealing has been a vital issue and the gas-sealing amorphous materials must be selected on the basis of the degree of thermal expansion matching between components and mechanical strength. In this respect, it is interesting to note that gas-sealing problems can be largely mitigated by using a single-chamber SOFC system since no separation between fuel and air is required [7–12].

In a SOFC system, computer simulation based on theoretical modelling is known to be a very efficient method to predict materials properties, reaction kinetics and unit cell performance. Theoretical modelling of SOFC can be divided into three parts. First, basic properties such as the ionic conductivity of electrolyte materials can be predicted by molecular dynamics or ab initio approaches [13–17]. Second, the reaction kinetics at the three-phase boundary (TPB) at the electrode can be simulated by micro modelling [18–21]. Third, a detailed understanding of the fluid dynamics, mass transport and heat conduction/convection in the SOFC system can be obtained through macro modelling. The overpotentials of individual SOFC cells can be successfully predicted through a series of macro modelling procedures [22–25].

In this study, fluid motion, diffusion of the fuel–air mixture and oxygen ion conduction is considered in the macro

* Corresponding author. Tel.: +82 2 2220 0507; fax: +82 2 2281 5308.
E-mail address: yongchae@hanyang.ac.kr (Y.-C. Chung).

0378-7753/$ – see front matter © 2005 Elsevier B.V. All rights reserved.
doi:10.1016/j.jpowsour.2005.03.229

Nomenclature

c_i	concentration of species i (kg m^{-3})
D_i	diffusivity of species i (m^2 s^{-1})
F	Faraday constant (C mol^{-1})
$[i]^{\text{channel}}$	concentration of species i at the gas channel (mol m^{-3})
i_e	current density (A m^{-2})
i_0	exchange current density (A m^{-2})
$[i]^{\text{TPB}}$	concentration of species i at three phase boundary (mol m^{-3})
M_i	molar weight of species i (kg mol^{-1})
$N_{0,i}$	inward mass flux of species i (kg m^{-2} s^{-1})
P	pressure in channel (Pa)
P_2	pressure in electrodes (Pa)
$P_{\text{N–S}}$	Pressure obtained from calculating the Navier–Stokes equation (Pa)
R	gas constant (J mol^{-1} K^{-1})
R_i	volumetric reaction rate of species i (kg m^{-3} s^{-1})
T	temperature (K)
u	velocity vector (m s^{-1})
u, v, w	x-, y-, z-components of velocity in channel (m s^{-1})
u_2, v_2, w_2	x-, y-, z-components of velocity in electrodes (m s^{-1})
v_i	stoichiometric coefficient of species i
V	voltage (V)
V_{act}	activation loss (V)
$V_{\text{con,a}}$	concentration loss in anode (V)
$V_{\text{con,c}}$	concentration loss in cathode (V)

Greek letters

α_a	charge transfer coefficient at anode
α_c	charge transfer coefficient at cathode
η	dynamic viscosity (Pa s)
κ	permeability (m^2)
ρ	density (kg m^{-3})
σ	conductivity (S m^{-1})

modelling scheme by using the three-dimensional finite element method (FEM). Next, ohmic loss, activation loss and concentration loss are obtained through a series of macro modelling procedures and, consequently, the performance characteristics of a micro single-chamber IT–SOFC are quantitatively investigated for various structural parameters.

2. Computational process

For the simulation, a Hibino B-type single-chamber SOFC [9,12] was employed (Fig. 1). The dimensions of the model for computer simulation are listed in Table 1.

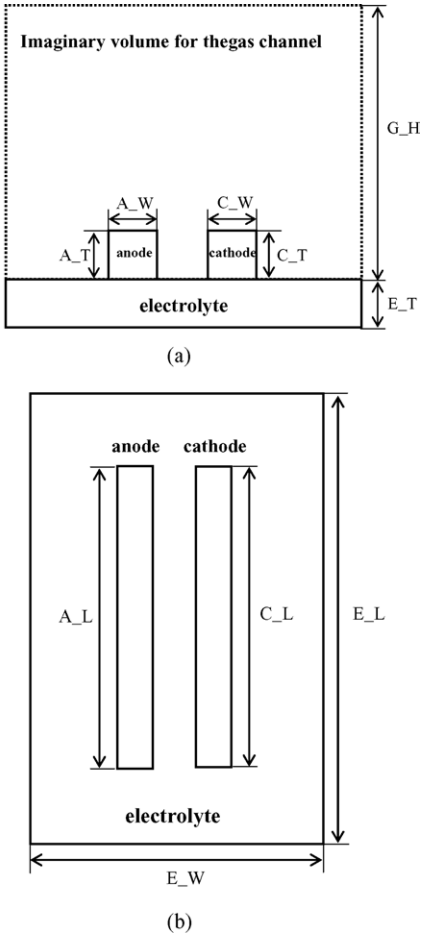

Fig. 1. Schematic diagram of calculation model based on Hibino B-type fuel cell [9,12]: (a) side view and (b) top view.

A fully dense and non-porous electrolyte was assumed and no penetration of gas species into the electrolyte was allowed. A NiO–$Ce_{0.9}Gd_{0.1}O_{1.95}$ (Ni–GDC) anode and a $Sm_{0.5}Sr_{0.5}CoO_3$–10%$Sm_2Ce_{0.8}O_{1.9}$ (SSC–10SDC) cathode with uniform pores of 100 nm diameter were designed to exhibit electronic and ionic conducting properties. It was also assumed that the oxidation of fuel in the gas mixture and the reduction of oxygen occurred only at the anode and at the cathode, respectively. The TPB, where the electrode reaction occurs, was assumed to be the interface between the

Table 1
Physical dimensions of micro single-chamber SOFC

Symbol	SOFC component	Dimension (μm)
E_L	Electrolyte length	1000
E_W	Electrolyte width	160
E_T	Electrolyte thickness	20
A_L	Anode length	900
A_W	Anode width	20
A_T	Anode thickness	20
C_L	Cathode length	900
C_W	Cathode width	20
C_T	Cathode thickness	20
G_H	Height of hypothetical gas channel	200

electrolyte and electrode, because most electrode reactions have been found [24] to take place within a 50 μm range in the interface region of the electrolyte and the electrode. In the present modelling, however, the TPB was assumed to be the whole electrode volume because the thickness of the electrodes was less than 50 μm.

For the simplicity, only hydrogen fuel was considered. The respective electrode chemical reactions can be represented by:

$$\text{Anode}: \quad 2H_2 + O_2 = 2H_2O + 4e^- \tag{1}$$

$$\text{Cathode}: \quad O_2 + 4e^- = 2O^{2-} \tag{2}$$

The injected fuel–air mixture was composed of hydrogen, nitrogen, oxygen and a small amount of water vapour and the temperature of the unit cell system was isothermally fixed at 773 K. A series of finite element calculations to find solutions for ionic conduction, fluid motion, diffusion and convection partial differential equations were carried by FEMLAB v3.1. The ohmic, activation and concentration losses were obtained from calculation of the voltage drop due to ionic conduction, finding the roots of the Butler–Volmer equation and determining the concentration distribution of each species resulting from the diffusion and convection in the anode, cathode and gas channel. The detailed procedure for modelling performance characteristics from loss calculations is depicted in Fig. 2. Finally, the theoretical open-circuit voltage (OCV) was obtained from the Nernst equation [26].

2.1. Ohmic loss

The ohmic loss is the voltage drop caused by the resistance of migrating oxygen ions and electrons in the electrodes. In this work, only ohmic loss from ionic conduction has been considered since that originating from electronic conduction is negligible. Using reported values of the conductivity (σ) of oxygen ions in the electrolyte [27] and the electrodes [27,28] at 773 K, Eq. (3) was solved, numerically and the voltage obtained.

$$-\nabla \cdot (\sigma \nabla V) = 0 \tag{3}$$

The boundary conditions applied to the calculation are given by Eqs. (4)–(6) for inward current density, outward current density and electrical insulation:

$$-\mathbf{n} \cdot (-\sigma \nabla V) = i_e \tag{4}$$

$$-\mathbf{n} \cdot (-\sigma \nabla V) = -i_e \tag{5}$$

$$-\mathbf{n} \cdot (-\sigma \nabla V) = 0 \tag{6}$$

2.2. Activation loss

The activation loss is due to overcoming the energy barrier when electrons released during the electrochemical reaction. Therefore, the activation loss depends on temperature, fuel species, electrode materials, oxygen partial pressure, etc. There are many different opinions of the nature oxidation and reduction mechanisms in SOFC electrodes, hence precise elucidation of multi-step electrochemical reactions are still remained unsolved [22]. The activation loss of IT–SOFC, however, becomes more critical compared with

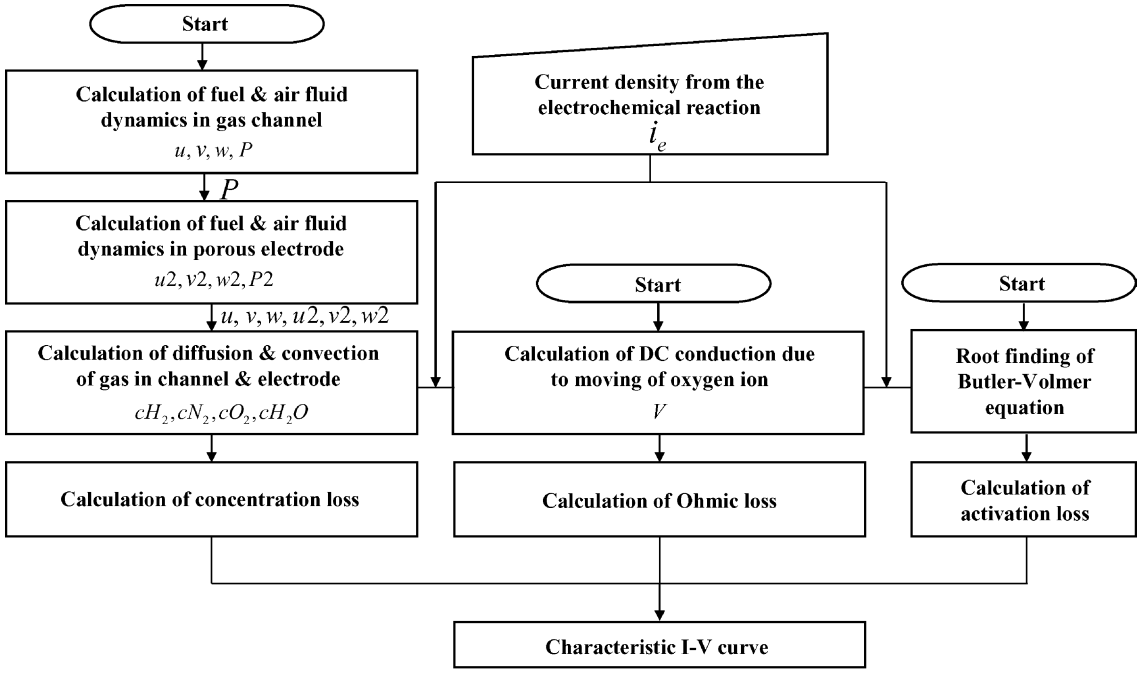

Fig. 2. Flow chart of performance characteristics analysis based on macro modelling.

high temperature–SOFCs. The Butler–Volmer Eqs. (7a) and (7b) represents the relation between activation loss and current density:

$$i_e = i_0 \left[\exp\left(\alpha_a \frac{FV_{act}}{RT}\right) - \exp\left(-\alpha_c \frac{FV_{act}}{RT}\right) \right] \quad (7a)$$

$$\alpha_a + \alpha_c = 1 \quad (7b)$$

Exchange current density (i_0), charge transfer coefficient (α_a and α_c) were referred to results of Zhu and Kee [22]. The numerical solution for the activation loss (V_{act}) was obtained by the Newton–Raphson method [29].

2.3. Concentration loss

Differences in the concentration of each species between the gas channel and the TPB lead to a concentration loss. In previous studies [24], the gas velocity in the porous electrodes was set to zero. In this work, however, convective diffusion was determined by calculating the velocity of gas fluid inside both electrodes. The inlet gas mixture was composed of H_2:N_2:O_2:H_2O = 0.5:0.38:0.105:0.0105 in mole fractions and assumed to obey the ideal gas law and amount of 180 sccm (H_2: 90 sccm, air: 90 sccm) was injected into the gas channel. To calculate the velocity distribution in the gas channel, the steady-state incompressible Navier–Stokes equation, Eq. (8a) with Eq. (8b) was solved numerically:

$$\rho(\mathbf{u}\cdot\nabla\mathbf{u}) - \nabla\cdot\eta(\nabla\mathbf{u} + (\nabla\mathbf{u})^T) + \nabla p = 0 \quad (8a)$$

$$\nabla\cdot\mathbf{u} = 0 \quad (8b)$$

The density (ρ) was calculated from the ideal gas law and the dynamic viscosity (η) of the fuel–air mixture was the molar mean value obtained from the product of individual viscosity and mole fraction. For setting-up boundary conditions, an initial gas velocity (u_0) of 42.47 m s^{-1} and a pressure (P_0) of 101325 Pa were applied to the gas inlet and outlet boundaries Eqs. (9) and (10). At the surface of electrolyte and electrode, no slip conditions were employed Eq. (11).

$$\mathbf{u}\cdot\mathbf{n} = \mathbf{u}_0 \quad (9)$$

$$\mathbf{n}\cdot(-\nabla\cdot\eta(\nabla\mathbf{u} + (\nabla\mathbf{u})^T) + \nabla P) = -\mathbf{n}P_0 \quad (10)$$

$$\mathbf{u} = 0 \quad (11)$$

To obtain the velocity distribution in the porous electrodes, Darcy's law equation (Eq. (12)) was solved with the calculated pressure values that resulted from solving the Navier–Stokes equation.

$$\nabla\cdot\left(\frac{-\kappa}{\eta}\nabla P\right) = 0 \quad (12)$$

The permeability (κ) of the anode and the cathode was assumed to be 1.0×10^{-12} m^2. The normal flux of the mixture gas was set to zero Eq. (13) at the interface between the electrolyte and the electrode and the pressure condition was applied to other boundaries of electrode. The resulting pressure values from fluid calculations at the gas channel were stored and used as a boundary value for the porous electrodes Eq. (14).

$$-\mathbf{u}\cdot\left(\frac{-\kappa}{\eta}\nabla P\right) = 0 \quad (13)$$

$$P = P_{N-S} \quad (14)$$

Finally, from the velocity distribution, the steady-state diffusion and convection equation, Eq. (15) was solved to obtain the concentration distribution of reactants and products in the gas channel and the electrodes.

$$\nabla\cdot(-D_i\nabla c_i + c_i\mathbf{u}) = R_i \quad (15)$$

The value of the diffusivity (D_i) of each species in the channel and porous media is given in Table 2. The diffusivity was calculated from the Hirschfelder model based on the Lennard–Jones potential [30]. In particular, when the diffusivity in the porous electrode was calculated, Knusen diffusion as well as the Bruggman model was considered to represent the actual porous media, which consisted of randomly distributed tortuous pores. The volumetric reaction rate (R_i) was defined as a mass quantity of reactants and products per unit volume per second, i.e.,

$$R_i = \pm\frac{\nu_i i_e}{4F} \times \text{area of reaction site (ARS)} \times \frac{1}{\text{electrode volume}} \times M_i \quad (16)$$

where R_i is positive if species i is the product (H_2O) and is negative if species i is the reactant (H_2, O_2); ν_i is the stoichiometric coefficient of reactions, i.e., $\nu_{H_2} = \nu_{H_2O} = 2$, $\nu_{O_2} = 1$. The area of the reaction site (ARS) can be calculated from the permeability.

The mass flux obtained from the density and the influx volume of the gas mixture was applied to the inlet boundary as a boundary condition Eq. (17). At the interface between the electrolyte and the electrodes, migration of each molecule across the interface should not be allowed Eq. (18). A convective flow condition was applied to the outlet boundary Eq. (19).

$$-\mathbf{n}\cdot(-D_i\nabla c_i + c_i\mathbf{u}) = N_{0,i} \quad (17)$$

$$-\mathbf{n}\cdot(-D_i\nabla c_i + c_i\mathbf{u}) = 0 \quad (18)$$

$$-\mathbf{n}\cdot(-D_i\nabla c_i) = c_i\mathbf{u}\cdot\mathbf{n} \quad (19)$$

Table 2
Diffusivity of each species at 773 K, 1 atm (cm^{2}s^{-1})

	Channel	Porous electrode
H_2	2.813	0.252
N_2	2.366	0.081
O_2	0.559	0.059
H_2O	0.757	0.079

From the calculated concentration distribution, the concentration loss was calculated through Eqs. (20) and (21) [22].

$$V_{\mathrm{con,a}} = \frac{RT}{4F}\left(2\ln\frac{[\mathrm{H_2}]^{\mathrm{channel}}}{[\mathrm{H_2}]^{\mathrm{TPB}}} - 2\ln\frac{[\mathrm{H_2O}]^{\mathrm{channel}}}{[\mathrm{H_2O}]^{\mathrm{TPB}}}\right) \quad (20)$$

$$V_{\mathrm{con,c}} = \frac{RT}{4F}\left(\ln\frac{[\mathrm{O_2}]^{\mathrm{channel}}}{[\mathrm{O_2}]^{\mathrm{TPB}}}\right) \quad (21)$$

3. Results and discussion

The calculated loss corresponding to variation in the current density is shown in Fig. 3a. As with other types of SOFC, the major loss originates from the ohmic loss caused by the diffusion of oxygen ions. On the other hand, the concentration loss is minimal due to the reduced concentration difference between the inside of the electrodes and the gas channel since whole volume of the electrodes served as reaction sites. The corresponding polarization curve, which is directly related to the performance of the SOFC, was obtained by subtracting all the calculated losses from the theoretical open-circuit voltage (1.133 V) (see Fig. 3b).

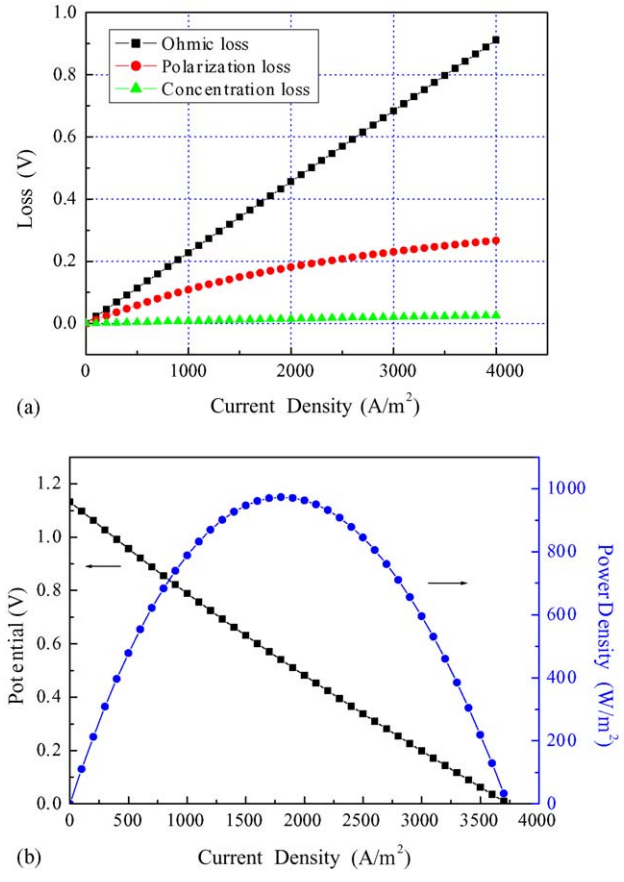

Fig. 3. (a) Predicted losses as current density variation. (b) Predicted polarization curve the distance between electrodes and the thickness of electrolyte is 20 and 20 μm, respectively.

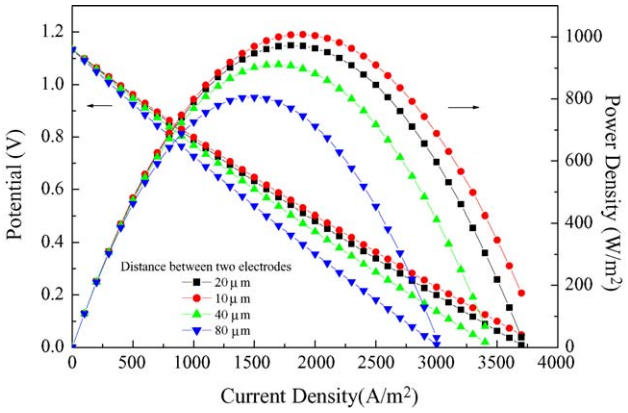

Fig. 4. Polarization curve corresponding to variation in the distance between two electrodes.

Next, the effect of the distance between the anode and the cathode on the polarization curve was quantitatively investigated (Fig. 4). On decreasing this distance, the power density of cell increases due to a reduction in ohmic loss. This agrees well with empirical expectation and is consistent with experimental reports [9,12].

The polarization curve according to variation in the thickness of the electrolyte is presented in Fig. 5. In contrast to a Hibino A-type single-chamber SOFC [9,12], the single-chamber SOFC adapted in this study (B-type) gives a higher power density with a thicker electrolyte. This is due to the ohmic loss behaviour according to variation in the thickness of the electrolyte (see Fig. 6). The ohmic loss decreases with increase in the thickness and converges at thicknesses above 80 μm. It can, therefore, be reasonably concluded that in the manufacturing step of a B-type single-chamber SOFC, a thicker electrolyte can be employed without deteriorating the performance characteristics, and no additional support materials for the required mechanical strength are required.

The effect of variation in the direction of the inflow gas mixture on the polarization curve is demonstrated in Fig. 7. The highest power density, is obtained when the gas mixture is injected into the vicinity of the cathode in a direction

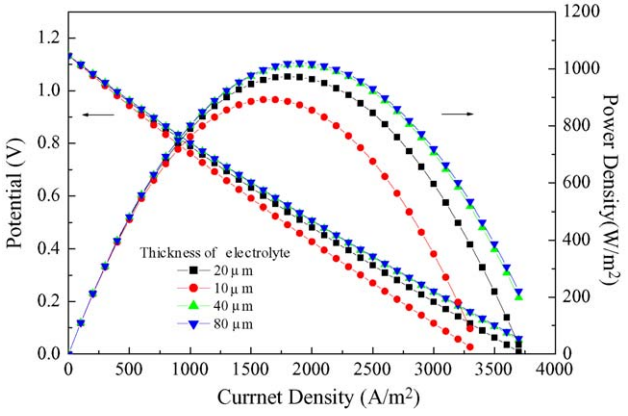

Fig. 5. Polarization curve for variation of the electrolyte thickness.

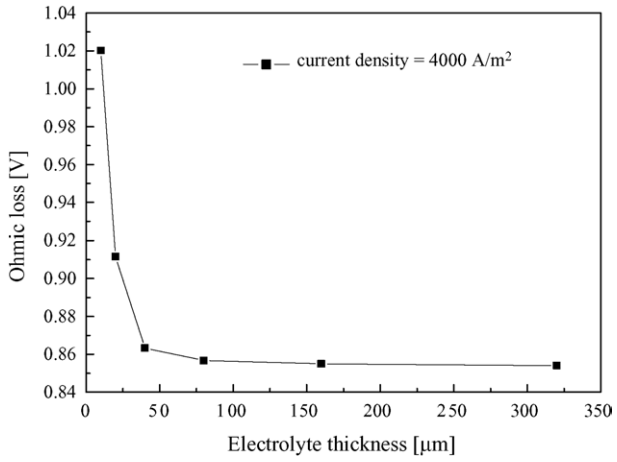

Fig. 6. Ohmic loss variation with electrolyte thickness.

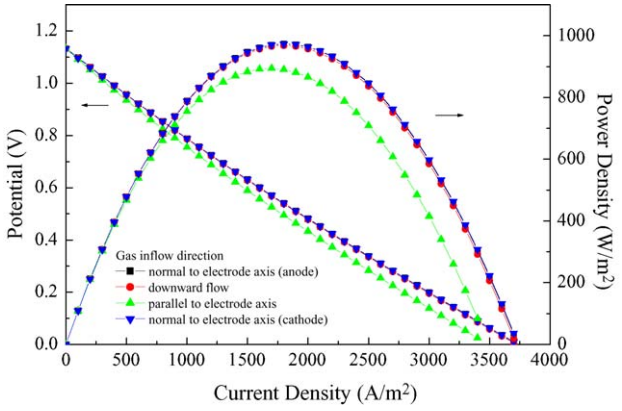

Fig. 7. Polarization curve for various inflow directions of fuel–air gas mixture.

perpendicular to the electrode axis. This observation can be understood by considering the diffusivity. The diffusivity of O_2 in the cathode is much lower than that of H_2 and H_2O in the anode, and, therefore, the migration of oxygen in the cathode is significantly retarded. By contrast, when inflow gas is injected into the cathode side, the velocity of gas in the cathode is higher than that in the anode. This increment of fluid velocity enhances the convective diffusion of oxygen in the cathode and, eventually, lowers the concentration loss. On the other hand, when the inflow gas direction is parallel to the electrode axis, the power density is predicted to be significantly lowered because the concentration difference of the gas species between the inlet and outlet regions of the SOFC system is extensive. This originates from the fact that the length of both electrodes is 45 times longer than the width and height.

4. Summary and conclusions

Computer simulation based on the macro modelling of multi-physical phenomena, e.g., ionic conduction, fluid dynamics and gas diffusion, has been successfully performed. Consequently, ohmic loss, polarization loss and concentration loss are quantitatively derived from the simulation results. The performance of a micro scale single-chamber SOFC system is found to be largely dependent on the structural parameters, the distance between the electrodes, the thickness of the electrolyte and the inflow direction of the gas mixture. In general, an improvement in performance can be obtained with a narrow interdistance between the electrodes and with a thicker electrolyte. When the inflow direction is perpendicular to the electrode axis, the specific micro single-chamber SOFC cell delivers the best performance. It is expected that the computational scheme developed in this study, can serve as an important guideline for manufacturing the micro single-chamber IT–SOFC system and for optimizing the performance characteristics.

References

[1] P. Sarkar, Fuel Cells Bull. 2003 (2003) 6.
[2] M. Lockett, M.J.H. Simmons, K. Kendall, J. Power Sources 131 (2004) 243–246.
[3] J.P.P. Huijsmans, F.P.F. Van Berkel, G.M. Christie, J. Power Sources 71 (1998) 107–110.
[4] K. Choy, W. Bai, S. Charojrochkul, B.C.H. Steele, J. Power Sources 71 (1998) 361–369.
[5] J.M. Ralph, A.C. Schoeler, M. Krumpelt, J. Mater. Sci. 36 (2001) 1161–1172.
[6] B.C.H. Steele, Solid State Ionics 134 (2000) 3–20.
[7] T. Hibino, A. Hashimoto, T. Inoue, J.-I. Tokuno, S.-I. Yoshida, M. Sano, Science 288 (16) (2000) 2031–2033.
[8] T. Hibino, Y. Kuwahara, S. Wang, J. Electrochem. Soc. 146 (1999) 2821–2826.
[9] T. Hibino, H. Tsunekawa, S. Tanimoto, M. Sano, J. Electochem. Soc. 147 (2000) 1338–1343.
[10] T. Hibino, A. Hashimoto, T. Inoue, J.-I. Tokuno, S.-I. Yoshida, M. Sano, J. Electochem. Soc. 147 (2000) 2888–2892.
[11] T. Hibino, A. Hashimoto, M. Yano, M. Suzuki, S.-I. Yoshida, M. Sano, J. Electochem. Soc. 149 (2002) A133–A136.
[12] T. Hibino, S. Wang, S. Kakimoto, M. Sano, Solid State Ionics 127 (2000) 89–98.
[13] H. Yoshida, T. Inagaki, K. Miura, M. Inaba, Z. Ogumi, Solid State Ionics 160 (2003) 109–116.
[14] H. Inaba, R. Sagawa, H. Hayashi, K. Kawamura, Solid State Ionics 122 (1999) 95–103.
[15] M.S. Khan, M.S. Islam, D.R. Bates, J. Mater. Chem. 8 (1998) 2299–2307.
[16] Y. Yamamura, S. Kawasaki, H. Sakai, Solid State Ionics 126 (1999) 181–189.
[17] T.P. Perumal, V. Sridhar, K.P.N. Murthy, K.S. Easwarakumar, S. Ramasamy, Physica A 309 (2002) 35–44.
[18] A.S. Ioselevich, A.A. Kornyshew, Fuel Cells 1 (2001) 40–65.
[19] S.H. Chan, Z.T. Xia, J. Electrochem. Soc. 148 (2001) A388–A394.
[20] M. Ihara, T. Kusano, C. Yokoyama, J. Electochem. Soc. 148 (2001) A209–A219.
[21] X.J. Chen, S.H. Chan, K.A. Khor, Electrochim. Acta 49 (2004) 1851–1861.
[22] H. Zhu, R.J. Kee, J. Power Sources 117 (2003) 61–74.
[23] E.H. Racheco, D. Singh, P.N. Hutton, N. Patel, M.D. Mann, J. Power Sources 138 (2004) 174–186.
[24] R. Suwanwarangkul, E. Croiset, M.W. Fowler, P.L. Douglas, E. Entchev, M.A. Douglas, J. Power Sources 122 (2003) 9–18.

[25] T. Ackmann, L.G.J. de Haart, W. Lehnert, D. Stolten, J. Electochem. Soc. 150 (2003) A783–A789.
[26] J. Larminie, A. Dicks, Fuel Cell Systems Explained, second ed., Wiley, 2003, pp. 35–42.
[27] B.C.H. Steele, Solid State Ionics 129 (2000) 95–110.
[28] C. Xia, W. Rauch, F. Chen, M. Liu, Solid State Ionics 149 (2002) 11–19.
[29] W.H. Press, S.A. Teukolsky, W.T. Vetterling, B.P. Flannery, Numerical Recipes in C, second ed., Cambridge University Press, 1992, pp. 362–367.
[30] J.R. Welty, C.E. Wick, R.E. Wilson, G. Rorrer, Fundamentals of Momentum, Heat and Mass Transfer, fourth ed., Wiley, 2001, pp. 431–444.